Numerical simulation of the long-term behaviour of a self-healing concrete beam vs standard reinforced concrete

T. Hazelwood,[a] A. D. Jefferson,[a] R.J. Lark,[a] D. R. Gardner[a]

[a]Cardiff School of Engineering, Cardiff University, Queen's Buildings, The Parade, Cardiff, CF24 3AA, Wales, UK

Correspondence to: A. D. Jefferson (JeffersonAD@Cardiff.ac.uk)

ABSTRACT

Research on the self-healing cementitious composite material system named LatConX is presented, with predictions made as to the effectiveness of the system in limiting crack widths in concrete beams subjected to sustained loads. A layered beam numerical model for the transient thermo-mechanical behaviour of reinforced concrete has been developed and coupled to a previously published numerical model for transient thermo-mechanical behaviour of a shape memory polymer. The combined model has been validated by comparison with experimental data. Finally, the model is used to predict ten-year crack widths in standard reinforced concrete beams, and in beams employing the LatConX system. These results indicate that the LatConX system has the potential to reduce crack widths by up to 65 % when compared with an identical beam without the LatConX system.

1. INTRODUCTION

This paper compares the predicted long-term behaviour of a new self-healing concrete material system with that of standard reinforced concrete. The new material system is named LatConX (LCX), it consists of both reinforcing steel and shape memory polymer (SMP) tendons included within a cementitious matrix. Once a beam has been cast, cured and loaded, the tendons' shrinkage process is triggered, applying a compressive force to the cementitious matrix. This compressive force has been shown to be beneficial to the cementitious matrix in three ways: it closes any cracks that have developed; it applies a compressive stress to the cracked faces, leading to improved healing of the cracks; and it improves the structural performance of the composite system by acting in the same manner as a prestressing system. This system has been described in more detail by Jefferson et al [1]. The SMP tendons are formed from the widely available polymeric material polyethylene terephthalate (PET).

A numerical model has been developed to facilitate the comparison between LCX and standard RC beams. The model is composed of a set of sub-models, which are combined in order to simulate the transient thermo-mechanical behaviour of reinforced concrete beams. The model accounts for all relevant material behaviour and their interactions. These include: mechanical damage, creep, shrinkage, thermal expansion/contraction, and self-healing of the cementitious matrix; mechanical behaviour of reinforcement; and transient thermo-mechanical behaviour of SMP tendons.

The model presented herein was developed with simplicity, ease of use, and robustness in mind; in particular, speed of convergence was a vital factor in the design of the model due to the large time scales under investigation.

Abbreviations
LCX - LatConX
SMP – Shape memory polymer
CDHM – Continuum damage healing mechanics
FPZ – Fracture process zone
SRC – Standard reinforced concrete

1.1. Material modelling of concrete

Most material models for concrete use either plasticity theory, damage mechanics or a combination of the two theories. Plasticity models require a yield surface, which is generally derived from a biaxial [2] or triaxial failure envelope, [3] [4], as well as a hardening/softening and flow rule. A number of effective plasticity models have been developed to simulate the nonlinear behaviour of concrete [5] [6] [7] although the natural weakness of plasticity theory, in this context, lies in its inability to simulate the stiffness degradation that accompanies physical micro-cracking in tension.

Damage mechanics provides a natural means of simulating the loss of stiffness due to micro-cracking [8] and a number of effective isotropic damage models have been developed for the simulation of damage in both tension and compression [9]–[12]. Anisotropic damage models have also been investigated extensively over the last thirty years, which include those developed by Simo and Ju, Carol et al, Borst and Gutierrez, and Desmorat et al [13],[14],[15],[16].

Many investigators have combined plasticity and damage theories to produce models that simulate both stiffness degradation and frictional behaviour, the latter of which is characterised by the development of permanent or plastic strains [17]–[22]

For the present work, a one dimensional damage approach has been adopted to simulate tensile cracking and a plasticity model has been used to simulate the behaviour of concrete in compression. This cementitious material model has been applied in a nonlinear layered beam model.

1.2. Healing

The self-healing behaviour of cementitious materials has received considerable attention in recent years. Comprehensive reviews have been published by several authors including those of Joseph et al, Wu et al, and Van Tittelboom & De Belie [23] [24] [25].

There has also been significant work, over the past two decades, on the development of material models for self-healing materials. Some of these models have been developed in relation to specific materials; for example, Miao and coworkers [26] presented a model for rock salt, while Mergheim and Stein [27] considered the behaviour of self-healing polymers. In addition, a number of generic self-healing models have been developed which are applicable to a range of materials [28]–[30]. The behaviour simulated by these models results from the healing of any microcracks (or macro-cracks) and microvoids present, a process which has been considered to be the opposite of damage, with healing sometimes being described as 'negative damage' [26],[28],[29]. This approach is often termed continuum damage healing mechanics (CDHM), a term originally coined by Barbero et al [28]. Furthering this concept, Voyiadjis and coworkers [30] developed a combined plasticity and CDHM model, including kinematic and isotropic hardening functions for plasticity, damage, and healing. Mergheim and Steinmann [27] developed a phenomenological model for self-healing polymers based on the assumption that healing is identical to negative damage. Their model is capable of simulating damage and healing processes simultaneously, and accounting for healing at non-zero strain.

A simple one-dimensional form of a healing model was presented by Schimmel and Remmers [29]. Their model is described in relation to discrete damage models however it can also be conveniently applied to the healing of continuum damage. The model allows a proportion of any damage present to be recovered due to healing at one time only; the progress of healing at this time is governed by a healing function, the form of which is chosen depending on the precise healing agent or process under consideration.

1.3. Modelling of creep and shrinkage in concrete

According to Bažant [31] there are two main model types for predicting the creep and shrinkage behaviour of concrete. There are true constitutive equations that simulate the real creep and shrinkage mechanisms and there are phenomenological models that approximate the mean behaviour of larger concrete elements.

The design models that appear in concrete codes of practice are generally of the latter type, of which examples include the ACI-209R-82 model [32], the B3 [33] and B4 [34] models, the CEB-FIP 1990 [35] models, GL2000 model [36], and Eurocode 2 [37]. Goel et al [38] presented a comparative study of five of these creep and shrinkage models in which they summarised the merits, and shortcomings of the models reviewed.

Bažant and coworkers [39],[40] developed a method for predicting concrete creep taking into account long-term aging and drying which has been termed solidification theory. A simplified version of a recently presented model [41], that uses some aspects of this solidification theory, has been developed for the present work. In this model, creep strains are predicted by a rheological model comprising multiple Maxwell elements in parallel. Creep strain predictions from Eurocode 2 [37] are also used to assess the accuracy of the computational creep model.

2. LatConX System Model

The non-linear numerical model developed to simulate the long-term behaviour of the LCX material system is illustrated in Figure 1. The model is composed of a number of elements; the exact configuration of which depends on the details of the LCX structure being considered. There are three different element types; continuum beam elements, fracture process zone (FPZ) elements and SMP bar elements. In all cases presented in this article, the model consists of two continuum beam elements either side of a central FPZ element, with the SMP element being incorporated as required. In this configuration, the model is applicable to situations in which either there is distributed time-dependent cracking along the beam, and/or there is a localised (dominant) crack at the centre of the beam. The latter, in particular, occurs in experimental beams that contain a central notch. The model in this form is considered adequate for all of the beam configurations considered in this paper; however, if required, the model could be applied with multiple FPZ elements and used to simulate a range of concrete beams types.

The model setup considered for all applications presented in this article is shown in Figure 1. This is a simply supported beam of length L, with a significant central notch, subjected to a centrally applied point load, P. The overall model comprises two continuum beam elements, each of length L_e, and a central FPZ of length w_c. The element that represents the PET tendon and the reinforcement layer are also shown in Figure 1

The fracture process zone width represents the physical zone over which micro-cracking occurs adjacent to a macro-crack and is normally assumed to be approximately three to five times the size of the coarse aggregate particles [42]. However, since the post-peak stress-strain relationship used in the FPZ element is scaled to w_c, as in Bažant and Oh's Crack-Band theory, the results are always highly insensitive to the value used for w_c [42].

A further note on the model is that cracking, creep and shrinkage are taken into account for the continuum elements using code based models, as explained in Section 2.3.

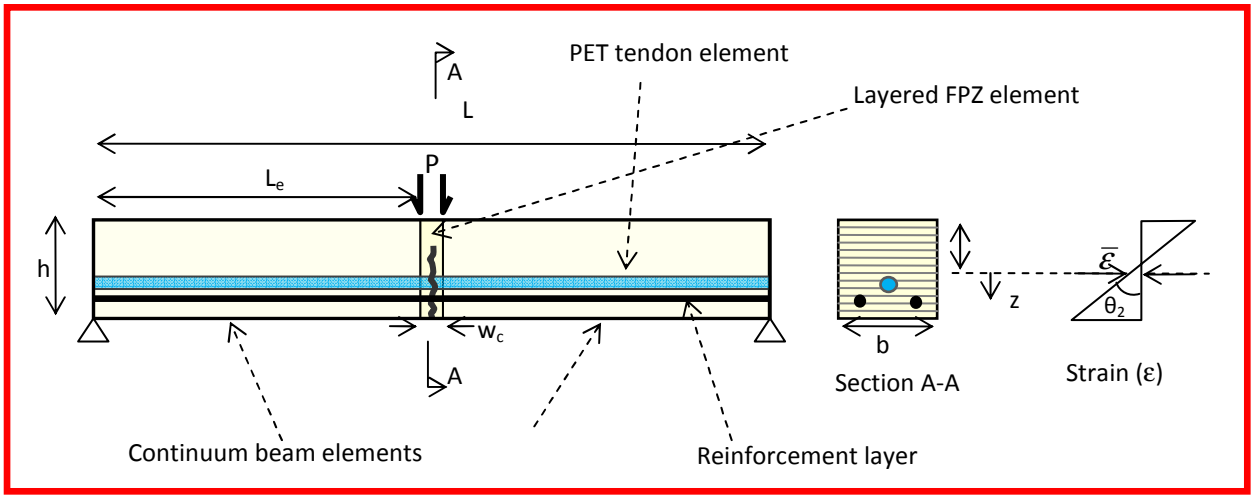

Figure 1 - Schematic diagram of numerical model

2.1. Nonlinear Fracture Process Zone

In this Section, the assumptions and relationships governing the behaviour of an FPZ element will be discussed. There are two key assumptions in the representation of an FPZ element:

1. Plane sections remain plane
2. The FPZ is subject to constant curvature

Using these assumptions, the total strain (ε_{tot}) at any level z in a beam section may be derived to be

$$\varepsilon_{tot} = \bar{\varepsilon} - \frac{2}{w_c} z \theta_2 \quad (1)$$

where $\bar{\varepsilon}$ is the mid-level reference strain, θ_2 the angle of rotation, and w_c is the width of the FPZ (see Figure 1). Using the relationship outlined in Equation 1, and the constitutive relationships for each material introduced in the following Sections, equilibrium equations may be established for the for FPZ element in terms of the rotation (θ_2) and axial strain at the reference height ($\bar{\varepsilon}$)

2.2. Constitutive Models

The behaviour of the concrete, steel, and polymer in this model are each governed by separate constitutive models, which are described below.

2.2.1. Mortar/concrete

The constitutive behaviour of mortar or concrete is simulated with the one-dimensional model shown in Figure 2. Tensile behaviour is governed by a uniaxial damage model, in which damage evolution is controlled by an exponential softening function. In the compression region, the behaviour is assumed to be elastic-perfectly plastic, as illustrated in Figure 2. It is acknowledged that this uniaxial compressive stress-strain relationship is a significant idealisation of the true behaviour of concrete and mortar, but since the focus of the paper is on cracking and healing, and not on ultimate behaviour, this idealisation is considered adequate for the present work.

The constitutive model also accounts for healing, creep, shrinkage, and thermal behaviour; the theories and resulting models governing these phenomena, as well as their integration with the basic mortar constitutive model, are described in the relevant sections below.

The effective mechanical strain ε_{efm}, which takes account of shrinkage, creep, and thermal strain is given by:

$$\varepsilon_{efm} = \varepsilon_{tot} - \varepsilon_{sh} - \varepsilon_{cr} - \varepsilon_{TH} \quad (2)$$

where; ε_{sh} is the shrinkage strain, ε_{cr} is the creep strain, and ε_{TH} is the thermal strain.

The constitutive equation for the tension zone is given by Equation (3).

$$\sigma = (1 - \omega) \cdot E \cdot (\varepsilon_{efm} - \varepsilon_{pl}) \quad (3)$$

in which σ is the axial stress in a beam layer, and ε_{pl} is the plastic strain, $\omega \in [0,1]$ is the damage parameter given by Equation (4) which is taken from Reference [20] and accounts for the loss of stiffness in the cementitious matrix resulting from microcracking, E is Young's modulus of the undamaged mortar/concrete, and ε_{efm} is the effective mechanical axial strain taking into account creep, shrinkage and thermal effects.

$$\omega = 0 \qquad \forall \ \zeta \leq \varepsilon_t \quad (4)$$

$$\omega = 1 - \frac{\varepsilon_t}{\zeta} e^{-c\frac{\zeta - \varepsilon_t}{\varepsilon_0 - \varepsilon_t}} \qquad \forall \ \zeta > \varepsilon_t$$

in which ε_t is the tensile strain limit, beyond which damage is initiated (i.e. $\varepsilon_t = \frac{f_t}{E}$), and ζ is the maximum historical value of the effective strain parameter, which is initialised to ε_t.

The strain at the effective end of the softening curve (ε_0) is computed from $\varepsilon_0 = \frac{u_0}{w_c}$, with u_0 being the crack opening displacement at the effective end of a stress-opening curve. u_0 is calculated from the specific fracture energy parameter as follows $u_0 \approx \frac{c \cdot G_f}{f_t}$.

The softening curve constant c is taken to be 5, as in reference [20].

The constitutive equation for the compression zone is given by Equation (5).

$$\sigma = E \cdot (\varepsilon_{efm} - \varepsilon_{pl}) \quad (5)$$

where E is Young's modulus of the mortar/concrete, noting that f_c in Figure 2, is the compressive strength of mortar/concrete.

$$\dot{\varepsilon}_{pl} = \dot{\varepsilon} \qquad \forall \quad \sigma = f_c$$

Equation (5) implies that any cracks present will close completely when the material goes into compression.

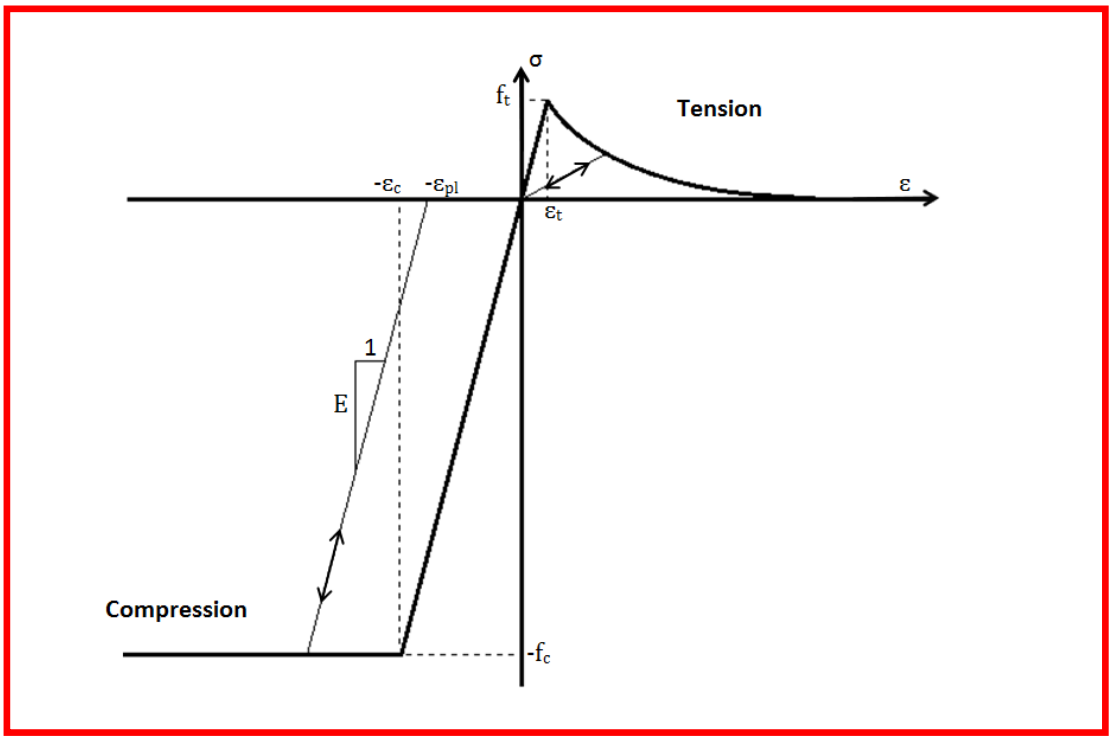

Figure 2 - Mortar constitutive model and primary variables

2.2.1.1. Shrinkage Strain

The shrinkage strain is calculated using Eurocode 2 [37]. In this code the shrinkage curve is calculated as a function of the environment's relative humidity, the mean compressive 28 day strength of the concrete, and the notional member size. It is noted that shrinkage is applied to both the continuum and FPZ elements.

2.2.1.2. Creep Strain

As mentioned above, a simplified version of the creep model developed by Jefferson et al [41] has been implemented for this work. This simplified model comprises of an elastic

spring and three Maxwell arms in parallel. Since the concrete stress is likely to vary through its depth, the creep strain is calculated separately for each layer of the FPZ element as a function of the stress applied to that layer.

The viscoelastic strain, $\varepsilon_{\mathrm{vec}}$, for each Maxwell arm is given by the standard solution shown in Equation (6).

$$\varepsilon_{\mathrm{vec_i}} = \varepsilon_{\mathrm{efc}}\left(1 - \mathrm{e}^{-\frac{\Delta \mathrm{t}}{\tau_c}}\right) + \varepsilon_{\mathrm{vec_{i-1}}}\left(\mathrm{e}^{-\frac{\Delta \mathrm{t}}{\tau_c}}\right) \quad (6)$$

where $\varepsilon_{\mathrm{efc}}$ is the effective strain on the creep unit (Equation (7)), $\Delta \mathrm{t}$ is the length of the time step being considered in seconds, i is the increment number, and τ_c is the relaxation time of the Maxwell arm.

$$\varepsilon_{\mathrm{efc}} = \varepsilon_{tot} - \varepsilon_{\mathrm{sh}} - \varepsilon_{\mathrm{TH}} - \varepsilon_{\mathrm{fr}} \quad (7)$$

in which $\varepsilon_{\mathrm{fr}}$ is the fracture strain, which is given by Equation (8).

$$\varepsilon_{\mathrm{fr}} = \omega(\varepsilon_{tot} - \varepsilon_{\mathrm{sh}} - \varepsilon_{\mathrm{TH}} - \varepsilon_{\mathrm{cr}}) \quad \text{if} \quad \varepsilon_{tot} - \varepsilon_{\mathrm{sh}} - \varepsilon_{\mathrm{TH}} - \varepsilon_{\mathrm{fr}} > 0 \quad (8)$$

$$\varepsilon_{\mathrm{fr}} = 0 \quad \text{otherwise}$$

The above equations allow the viscoelastic strain for each Maxwell arm to be calculated, and these are combined into a single total creep strain for each FPZ element layer. The contribution of each Maxwell arm to this total creep strain is controlled by a set of weighting factors, β_{ci}. The total creep strain in the FPZ element is then given by;

$$\varepsilon_{\mathrm{cr}} = \sum_{\mathrm{i}=2}^{4} \beta_{c_{\mathrm{i}}} \varepsilon_{\mathrm{vec_i}} \quad (9)$$

where β_{ci} is the weighting factor for arm i, and $\varepsilon_{\mathrm{veci}}$ is the viscoelastic strain for each arm. The values of β_c and τ_c for each arm were set by calibrating against the creep model presented in Eurocode 2 [37] for the desired environmental conditions.

An example calibration curve and the relevant β_c and τ_c values can be seen in Table 1 and Figure 3.

This creep model is only applied to the FPZ element. A simplified, code-based, approach is used for the continuum beam elements, as explained in section 2.3.

Table 1 – β_c and τ_c values used for example creep calibration curve

Arm No	1	2	3	4
β_c	0.2	0.5	0.26	0.04
τ_c (days)	NA	0.6	50	2000

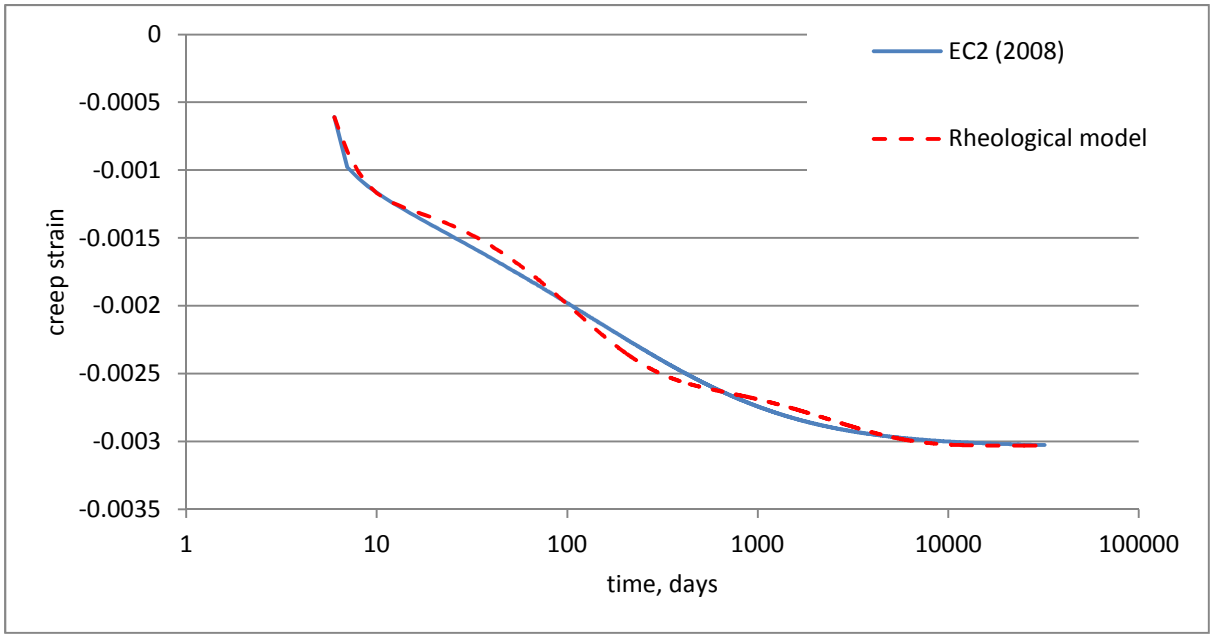

Figure 3 – Example calibration curve. Compressive strength = 30 N/mm^2, dimensions 300 x 450 mm, relative humidity 50 %, loaded at 7 days

2.2.1.3. Thermal Strain

It is normal practice to assume that the component of early thermal cracking associated with the heat of hydration occurs due to cooling from the peak hydration temperature (Bamford 2007 CIRIA guide and BD28/87). The thermal strain (ε_{TH}) that gives rise to such cracking may be calculated as follows (BD28/87)

$$\varepsilon_{TH} = -0.8\alpha_c(T_1 + T_2) \quad (10)$$

where α_c is the coefficient of thermal expansion for concrete, taken as 12 x 10^{-6}, and T_1 and T_2 are anticipated temperature decreases from the hydration peak. The values of T_1 and T_2 are determined in accordance with BD28/87; T_1 is the short term fall in temperature from the hydration peak, and T_2 is the long term fall in temperature from ambient to the seasonal minimum.

In the present model, the thermal strain is applied at time, t_{TH}, which is before any other creep, shrinkage, or applied load effects are applied. This approach is considered adequate for the simulations reported in this paper.

2.2.1.4. Self-Healing

Post-damage strength regain, in the form of self-healing, is also accounted for in the mortar/concrete constitutive model. This strength regain could either be due to the action of healing additives or autogenous healing within the cementitious matrix. Hence, the degree of self-healing varies depending on the exact nature of the healing phenomenon considered.

The healing model is similar to that of Schimmel and Remmers [29] however, instead of the healing progressing according to a healing function, it is assumed to occur instantaneously. Thus, there are just two parameters to consider; the time of healing (t_H) and the percentage of current damage regained ($H \in [0,1]$). Healed material is considered to form in a stress free state and thus the strain given by Equation (2) at the time that healing is applied (ε_H) is recorded and employed in equation (13). The level of damage at the time of healing (ω_H) is also recorded and included in the expression for the stress in the healed material, σ_H, given in Equation (11). The inclusion of ω_H results in the level of healing being proportional to the existing level of damage at the time of healing.

$$\sigma_{\mathrm{H}} = \mathrm{H} \cdot \omega_{\mathrm{H}} \cdot \mathrm{E}_{H} \cdot \left(\varepsilon_{efm} - \varepsilon_{\mathrm{H}}\right) \quad (11)$$

where Young's modulus $\mathrm{E_H}$ of the healed mortar/concrete is a function of any strain applied to the material beyond the strain at healing i.e. ε-ε_{H}.

Combining Equations (3) or (5), and (11) gives the total stress-strain relationship for the mortar/concrete shown in Equation (12).

$$\sigma_{\mathrm{total}} = \sigma + \sigma_{\mathrm{H}} \quad (12)$$

2.2.2. Reinforcing Steel

The trilinear constitutive model governing the behaviour of the reinforcing steel is displayed in Figure 4.

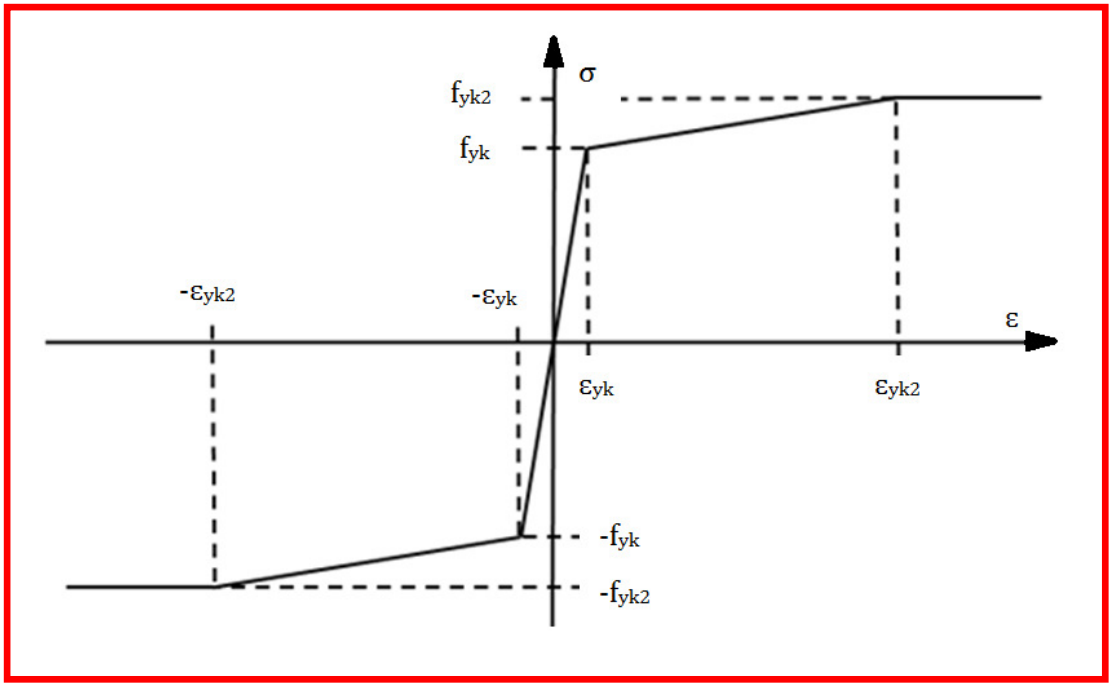

Figure 4 - Reinforcing steel constitutive model

It is assumed that there is no slip between the cementitious matrix and the reinforcing steel, and therefore the strains applied to reinforcement elements are the total strains at the relevant level in the beam, obtained from Equation (1). This assumption is acceptable when the applied load considered does not exceed the anticipated working load level [43].

In all of the examples presented in this article, the steel reinforcement material parameters are as shown in Table 2.

Table 2 – Material parameters for steel reinforcement

ε_{yk}	f_{yk}	ε_{yk2}	f_{yk2}
0.0029	500 MPa	0.2480	653 MPa

2.2.3. Polymer Tendons

2.2.3.1. Constitutive Model

The constitutive behaviour of the SMP tendons is governed by a transient thermo-mechanical model developed previously [44]. The constitutive model is composed of a number of rheological elements (Figure 5).

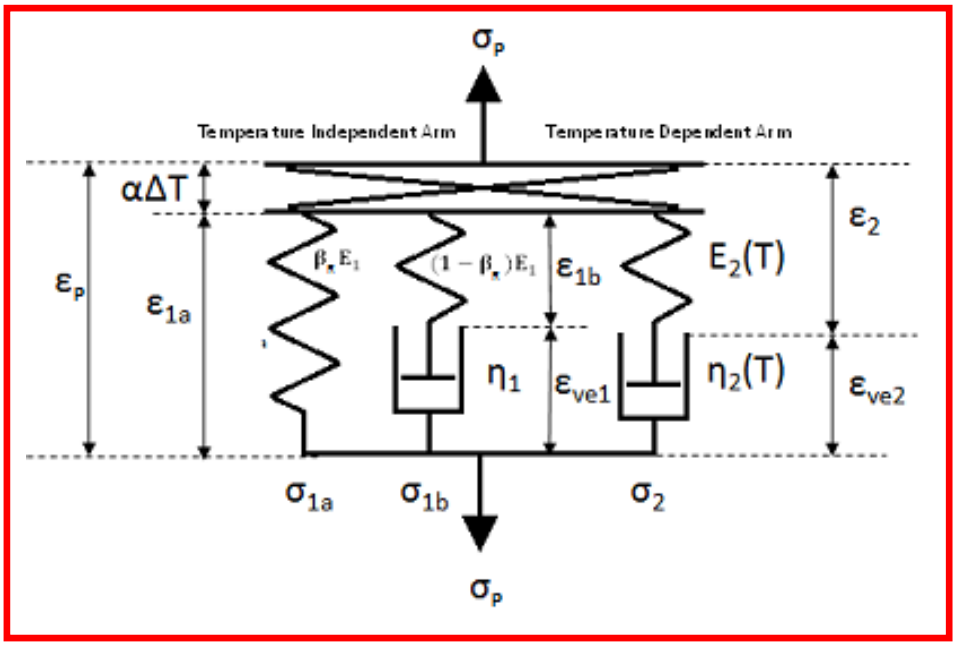

Figure 5 – Rheological representation of polymer constitutive model

The stress in the polymer (σ_p) is given by Equation (13).

$$\sigma_p = \beta_R \cdot E_1 \cdot \varepsilon_p + (1-\beta_R) \cdot E_1 \cdot (\varepsilon_p - \varepsilon_{ve1}) + E_2(T) \cdot (\varepsilon_p - \varepsilon_{ve2}) - (E_1 + E_2(T)) \cdot \alpha \cdot (T - T_{ambient}) \quad (13)$$

in which ε_p, ε_{ve1}, ε_{ve2}, E_1, E_2, are the strains, and material properties for each arm of the model, as shown in Figure 5, β_R is the weighting factor for long term behaviour, T is the current temperature, $T_{ambient}$ is the ambient temperature, and α is the coefficient of thermal expansion.

For each time increment (j) the viscoelastic strains (ε_{ve1}, ε_{ve2}) are updated according to the relationship in (14).

$$\varepsilon_{ve_j} = \varepsilon_{\theta_j}\left(1 - e^{-\Delta t/\tau}\right) + \varepsilon_{ve_{j-1}}.e^{-\Delta t/\tau} \quad (14)$$

in which ε_θ is the overall strain on the model at the midpoint of the time increment i.e. θ = 0.5, Δt is the size of the time step i.e. t_j-t_{j-1}, and $\tau = \eta/E$.

2.2.3.2. Combination with Beam Model

For each time increment, the stress in any polymer tendon is computed on the assumption that it is restrained at a length equal to that of the beam at the level of the polymer tendon, (z_p). This restraining length is denoted L_R and is calculated according to Equation (15).

$$L_R = L + \Delta L \quad (15)$$

in which L is the original length of the beam, and ΔL is the change in length of the beam which is contributed to by the displacements of both of the continuum beam elements (ΔL_{Le}) and the FPZ (ΔL_{FPZ}). In the FPZ, the sum of all contributing strains at any level is given by Equation (1), thus the total displacement at the level of the polymer tendon is:

$$\Delta L_{FPZ} = \bar{\varepsilon} w_c - 2\theta_2 z_p \quad (16)$$

The displacement in the two continuum beam elements is that shown in (17) which accounts for axial and rotational displacements in the elements due to applied moment, stress in the polymer, shrinkage, creep, and thermal strains.

$$\Delta L_{Le} = 2L_e\left[\frac{A_p\sigma_p}{AE_{cef}(t)} + \frac{z_p}{E_{cef}(t)I_{int}(M_{max})}\left[A_p\,\sigma_p z_p + \frac{M}{2}\right] + [\varepsilon_{sh} + \varepsilon_{TH}]\left[\frac{AE_{cef}(t)}{A_s E_s + AE_{cef}(t)} + \frac{\alpha_e S z_p}{I_{int}(M_{max})}\right]\right] \quad (17)$$

in which A_p is the cross sectional area of the polymer tendon, σ_p is the stress in the polymer tendon at the end of the previous time increment, A is the concrete area, $E_{cef}(t)$ is the effective concrete Young's modulus as a function of time, which accounts for creep behaviour in the continuum elements (see Equation (20)), M is the applied moment, and $I(M_{max})$ is the second moment of area of the beam as a function of the maximum historical applied moment, M_{max}, A_s is the total area of reinforcement, E_s is Young's modulus of the reinforcement, α_e is the modular ratio, and S is the first moment of area of the reinforcement. The model allows for cracking in the continuum beam elements in an averaged sense by using an inertia interpolated between a cracked and an uncracked state, as explained in section 2.3.

An overall strain applied to the polymer is derived from this change in length and substituted into the stress strain relationship of Equation (13). In which, $\varepsilon_p = (L_R - L_{pmin})/L_{pmin}$, $L_{pmin} = L/(1+\varepsilon_{p0})$, and ε_{p0} is the drawing strain used in the polymer manufacturing process, the value for this comes from the polymer constitutive model [44].

2.3. Continuum beam Elements

In the model setup considered throughout this publication, one continuum beam element is located on either side of the central FPZ.

The continuum beam elements are Bernoulli-Euler beam elements with nonlinear constitutive relationships that take account of cracking, creep, and shrinkage. The standard secant stiffness relationship for these elements is given by Equation (18).

$$\begin{bmatrix} F_1 \\ M_1 \\ F_2 \\ M_2 \end{bmatrix} = \frac{E_{cef}(t) \cdot I_{int}(M)}{L_e} \begin{bmatrix} 12/L_e^2 & 6/L_e & -12/L_e^2 & 6/L_e \\ 6/L_e & 4 & -6/L_e & 2 \\ -12/L_e^2 & -6/L_e & 12/L_e^2 & -6/L_e \\ 6/L_e & 2 & -6/L_e & 4 \end{bmatrix} \begin{bmatrix} w_1 \\ \theta_1 \\ w_2 \\ \theta_2 \end{bmatrix} \quad \textbf{(18)}$$

The approach from Eurocode 2 [37] has been used to determine the effective cracked second moment of area (I_{int}) and effective Young's modulus (E_{cef}) of the beam sections, the expressions for these are:

$$I_{int} = (1 - \delta)I_{un} + \delta \cdot I_{cr} \quad (19)$$

$$E_{cef} = \frac{E}{\varphi + 1} \quad (20)$$

in which I_{int} is the interpolated value of the second moment of area, δ is a distribution factor used to take account of tension stiffening of a reinforced concrete section, I_{un} and I_{cr} are the uncracked and cracked second moments of area respectively, and φ is the creep factor determined in accordance with Eurocode 2 [37].

Shrinkage in the continuum beam elements has been accounted for by calculating a curvature due to shrinkage according to Equation (21).

$$\frac{1}{r_{cs}} = \varepsilon_{sh}\alpha_e \frac{S}{I_{int}} \quad (21)$$

in which r_{cs} is the radius of curvature due to shrinkage.

2.4. Assembly of equilibrium equations for FPZ

The FPZ behaviour is modelled using a layered approach in which the beam is divided into a number of discrete layers (n_{lay} – usually 100). Each layer has an effective width and depth of b and Δz respectively. The strain in each layer is computed using Equation (1). The effect of any reinforcement is accounted for in the same manner by adding its contribution to the overall axial and bending stiffness as a function of the reinforcement's area, depth within the beam, and axial stiffness, according to the constitutive model presented in Figure 4. Thus, the internal axial force, N, and moment, M, for a reinforced concrete section subjected to a total strain at a specified reference height, $\bar{\varepsilon}$, and rotation, θ_2 are given by (22) and (23) respectively.

$$N = \sum_{i=1}^{nlay} (1 - \omega) E \varepsilon_{efm_i} b_i \Delta z_i + \sum_{i=1}^{nlay} (1 - \omega_2) \omega_H H E \left(\varepsilon_{efm_i} - \varepsilon_{H_i}\right) b_i \Delta z_i + \sum_{i=1}^{nrebar} E_s \varepsilon_i A_{s_i} \quad (22)$$

$$M = \sum_{i=1}^{nlay} (1 - \omega) E \varepsilon_{efm_i} b_i z_i \Delta z_i + \sum_{i=1}^{nlay} (1 - \omega_2) \omega_H H E \left(\varepsilon_{efm_i} - \varepsilon_{H_i}\right) b_i z_i \Delta z_i + \sum_{i=1}^{nrebar} E_s \varepsilon_i A_{s_i} z_{r_i} \quad (23)$$

in which z_i and z_{ri} are the depths for each mortar/concrete or reinforcement layer respectively relative to the reference height; the damage parameters ω and ω_2 for each layer are a function of ε_{efmi} and $(\varepsilon_{efmi} - \varepsilon_{Hi})$ respectively; and A_{si} is the area of steel in each reinforcement layer.

ε_i, and ε_{efmi} are the strains at the centre of each layer, as given by Equations (24) and (25), which are discretised forms of Equations (1) and (2).

$$\varepsilon_i = \bar{\varepsilon} - \frac{2}{w_c} z_i \theta_2 \quad (24)$$

$$\varepsilon_{efm_i} = \varepsilon_i - \varepsilon_{sh} - \varepsilon_{cr_i} - \varepsilon_{TH} \quad (25)$$

Combining Equations (22), (23), (24), and (25); equating (22) to the load from the polymer tendon, if present, and (23) to the externally applied moment, leads to a system of equilibrium equations for the FPZ as shown in Equation (26).

$$\mathbf{F} = [\boldsymbol{\Omega}] \cdot [\mathbf{u}] \quad (26)$$

in which $\mathbf{F}$, $\boldsymbol{\Omega}$, and $\mathbf{u}$ are represented by the following:

$$F = \begin{bmatrix} \sigma_p A_p + \sum_{i=1}^{nlay} b_i \Delta z_i E \left((1 - \omega_i)(\varepsilon_{TH} + \varepsilon_{sh} + \varepsilon_{cr_i}) + (1 - \omega_{2_i}) \omega_{H_i} H (\varepsilon_{TH} + \varepsilon_{sh} + \varepsilon_{cr_i} + \varepsilon_{H_i})\right) \\ M_{ap} + \sigma_p A_p z_p + \sum_{i=1}^{nlay} b_i z_i \Delta z_i E \left((1 - \omega_i)(\varepsilon_{TH} + \varepsilon_{sh} + \varepsilon_{cr_i}) + (1 - \omega_{2_i}) \omega_{H_i} H (\varepsilon_{TH} + \varepsilon_{sh} + \varepsilon_{cr_i} + \varepsilon_{H_i})\right) \end{bmatrix}$$

$$\Omega = \begin{bmatrix} \sum_{i=1}^{nlay} b_i \Delta z_i E \left((1 - \omega_i) + (1 - \omega_{2_i}) \omega_{H_i} H\right) + \sum_{i=1}^{nrebar} E_s A_{s_i} & \frac{-2}{w_c} \left[\sum_{i=1}^{nlay} b_i z_i \Delta z_i E \left((1 - \omega_i) + (1 - \omega_{2_i}) \omega_{H_i} H\right) + \sum_{i=1}^{nrebar} E_s A_{s_i} z_{r_i}\right] \\ \sum_{i=1}^{nlay} b_i z_i \Delta z_i E \left((1 - \omega_i) + (1 - \omega_{2_i}) \omega_{H_i} H\right) + \sum_{i=1}^{nrebar} E_s A_{s_i} z_{r_i} & \frac{-2}{w_c} \left[\sum_{i=1}^{nlay} b_i {z_i}^2 \Delta z_i E \left((1 - \omega_i) + (1 - \omega_{2_i}) \omega_{H_i} H\right) + \sum_{i=1}^{nrebar} E_s A_{s_i} {z_{r_i}}^2\right] \end{bmatrix}$$

$$u = \begin{bmatrix} \bar{\varepsilon} \\ \theta_2 \end{bmatrix}$$

2.5. Summary of material parameters

Due to the large number of material parameters required for the constitutive models described in this article, a summary table has been provided (Table 3), which describes each parameter, gives typical values, and provides some guidance on how the parameter should be determined.

Table 3 – Summary of material parameters

Symbol	Description	Typical Value	Comments
Concrete Material Parameters			
w_c	Length of fracture process zone	100 mm	3-5x coarse aggregate size.
E	Young's modulus of mortar/concrete	20 – 35 kN/mm^2	Standard material constant.
c	Stress-opening curve constant	5	This defines the slope and extent of the softening portion of the stress-strain curve for mortar/concrete in the tension regime (Figure 2). The value of 5 has been used as in reference [20].
G_f	Specific fracture energy of mortar/concrete	0.1 N/mm (0.025 for mortar)	Standard material constant.
f_t	Tensile strength of mortar/concrete	2.9 N/mm^2	Standard material constant.
f_c	Compressive strength of mortar/concrete	30-40 N/mm^2	Standard material constant.
τ_{ci}	Relaxation time for each Maxwell arm of the creep model	Widely varied	Set by calibration against the Eurocode 2 method.
β_{ci}	Creep model weighting factor	Widely varied	This governs the weight of contribution of each Maxwell arm viscoelastic strain to the total creep strain. The values are set by calibration with Eurocode 2 equations.
T_1	Short term fall in temperature for mortar/concrete from hydration peak	28°C	Design value taken from BD28/87 – assuming plywood formwork and Summer construction.

T_2	Long term fall in temperature from ambient to the seasonal minimum for mortar/concrete	0°C	Design value taken from BD28/87 – Beam is less than 15m in length.
α_c	Coefficient of thermal expansion for mortar/concrete	$12x10^{-6}$	Standard material constant.
t_{TH}	Time of application of thermal strain	3 days	Thermal strain of this nature occurs soon after casting (before the application of any load); providing this criterion is satisfied, the precise time has no effect on the solution.
t_H	Time of healing	Problem dependent	This depends on the nature of healing being considered.
H	Healing parameter	Problem dependent	Percentage of level of damage at $t=t_H$ that is healed.
Polymer Material Parameters			
σ_{res}	Manufacturing drawing stress	25-30 MPa	Determined in material tests, described by Hazelwood at al [44], and Dunn et al [45]
β_R	Relaxation weighting factor for temperature independent	0.95-0.99	
τ_p	Relaxation time for temperature independent arm	200000 seconds	
E_{tot}	Ambient temperature Young's Modulus	6000 MPa	
α	Coefficient of thermal expansion	$10^{-4.8}$	
E_{TH}	High temperature Young's modulus	845 MPa	
T_{LE}	Lower bound for thermal transition of Young's modulus	70°C	
T_{HE}	Upper bound for thermal transition of Young's modulus	120°C	
b_p	Material constant governing temperature dependent material property functions	3.3	
c_p	Material constant governing temperature dependent material property functions	5	
d_p	Material constant governing temperature dependent material property functions	1.2	
f_p	Material constant governing temperature dependent material property functions	0.1	
η_{2L}	High temperature viscosity for temperature dependent arm	$3.122x10^7$ P	
η_{2H}	Low temperature viscosity for	$1.575x10^4$ P	

	temperature dependent arm		
$T_{L\eta}$	Lower bound for thermal transition	30°C	
$T_{H\eta}$	Upper bound for thermal transition	90°C	
Steel Material Parameters			
ε_{yk}	Initial yield strain for steel reinforcement	0.0029	Standard material constant.
ε_{yk2}	Final yield strain beyond which hardening behaviour ceases for steel reinforcement	0.2480	Standard material constant.
f_{yk}	Initial yield stress for steel reinforcement	500 MPa	Standard material constant.
f_{yk2}	Final yield stress beyond which hardening behaviour ceases for steel reinforcement	653 MPa	Standard material constant.

2.6. Model Algorithms

The overall algorithm for simulating the long term behaviour of a structural element is outlined below, with further algorithms for specific parts of the model being given in Appendix A.

2.6.1. Main algorithm defining details for analysis

1	(is, t, T, ε_{ve1}, ε_{ve2}, ε_p, M, ε_{bar}, θ_2, ε_L, ζ, ε_{sh}, ε_{cr}, ε_{vec}, σ_p, ε_H, ω_H, ε_{LH}, ζ_H) = 0	*Initialise all variables and counters*
2	while t < t_{TH} is = is + 1, t = t + Δt (T, ε_{ve1}, ε_{ve2}, ε_p, M, ε_{bar}, θ_2, ε_L, ζ, ε_{sh}, ε_{cr}, ε_{vec}, σ_p, ε_H, ω_H, ε_{LH}, $\zeta_H)_{is}$ = (T, ε_{ve1}, ε_{ve2}, ε_p, M, ε_{bar}, θ_2, ε_L, ζ, ε_{sh}, ε_{cr}, ε_{vec}, σ_p, ε_H, ω_H, ε_{LH}, $\zeta_{Hprev})_{is-1}$	*Time dependent processes are assumed to begin at t = t_{TH} thus update counters and set variables up to this point*
3	if t = t_{TH} Set ε_{TH}	*Apply thermal strain at t = t_{TH}* *See Equation (10).*
4	See iterative solver algorithm in Appendix A	*Compute updated beam configuration for thermal strain*
5	See time step algorithm in Section 2.6.2	*Simulate time dependent processes and compute updated beam configuration for each time step up until time of loading, t_0*
6	Δt = 0, $\Delta M = \frac{M_{ap}}{n_{step}}$ See iterative solver algorithm in Appendix A	*Incrementally apply permanent moment and compute beam configurations throughout*
7	See time step algorithm in Section 2.6.2	*Simulate time dependent processes and compute updated beam configuration for each time step up for required length of time I.e. up to t_{final}*

2.6.2. Algorithm for each time step

1	t, T, ε_{ve1}, ε_{ve2}, ε_p, M, ε_{bar}, θ_2, ε_L, ζ, ε_{sh}, ε_{cr}, ε_{vec}, σ_p, ε_H, ω_H, ε_{LH}, ζ_H	*Input all values from previous time step*
2	is = is + 1	*Update counters*
3	t = t + Δt , T = T + ΔT	*Set conditional changes for time step*
4	See creep algorithm in Appendix A	*Update creep strains*
5	See shrinkage algorithm in Appendix A	*Update shrinkage strains*
6	See polymer algorithm in Appendix A	*Update polymer state*
7	See iterative solver algorithm in Appendix A	*Compute updated beam configuration*

3. EXAMPLES

The data from two experimental programs have been used to validate the numerical model. In the examples that follow, healing has not been considered unless stated otherwise.

3.1. Example 1

This example considered experimental data from Jefferson et al [1]. This test series used hollow prismatic mortar beams with SMP tendons fixed within; the beam cross-sections were 25mm square with a central 10mm square void. These samples were first mechanically tested 4 days after casting, with the polymer in its pre-activated state, thus providing no resistance to the applied load. Next, the samples were heated to 90℃ and soaked at this temperature for 18 hours, in order to activate the shrinkage process of the polymer tendons. The specimens were then mechanically tested for a second time 4 days later (8 days after casting) i.e. with the restrained activated polymer contributing to the load deflection behaviour. During both the test at 4 days and the test at 8 days, the fracture-softening behaviour was recorded. With the exception of the healed parameter (H) the material properties of the mortar were determined from material tests carried out by Jefferson et al. Both the mean value and coefficient of variation for each material property found in these materials tests are displayed in Table 4, with the mean value being used in the numerical predictions. H has been set by experimental calibration to the 8 day test data. The creep parameters for the FPZ element are shown in Table 5. No thermal strain is applied in this

example since the beams were not considered to be under any significant restraint during the period of cooling from the maximum heat of hydration.

Table 4 - Material parameters for example 1

	E kN/mm^2	E_p kN/mm^2	A_p mm^2	σ_{res} N/mm^2	w_c mm	f_c N/mm^2	f_t N/mm^2	H	G_f N/mm
Mean	24.8	6.0	20.7	33.8	5	19.5	2.0	0.005	0.025
CoV %	*1.6*	*2.5*	-	*2.3*	-	*8.3*	*7.3*	-	*11.7*

Note: f_c is taken as 0.85*f_{cu}, where f_{cu} was the strength obtained from 40mm cubes; E_p is the total Young's modulus for the polymer i.e. $E_1 + E_2$ in the numerical model.

Table 5 – Parameters used in creep model for all example and long term simulations

		Arm 1		Arm 2		Arm 3		Arm 4	
		β	τ	β	τ	β	τ	β	τ
Example 1		0.08	NA	0.84	0.5	0.07	100	0.01	2000
Example 2	Beams	0.3		0.35	1.2	0.25	40	0.1	1000
	Slabs	0.17		0.67	1.6	0.14	110	0.02	2200
Long term Eurocode Simulation		0.2		0.5	0.6	0.26	50	0.04	2000

Figure 6 shows the comparison between the experimental data and the model predictions, in terms of the applied load and the crack mouth opening displacement (CMOD), using the material properties from Table 4, and it can be seen that the numerical predictions closely match the experimental data. It should be noted that in this example the importance and impact of the healing parameter is minimal (0.5 % strength regain): this parameter becomes more important when a more complete self-healing concrete system is considered, i.e. one which combines the expected crack closure capability of LatConX with a healing additive agent that aids strength regain. It is anticipated that further research will lead to a better understanding of the level of strength regain expected for different types of healing system.

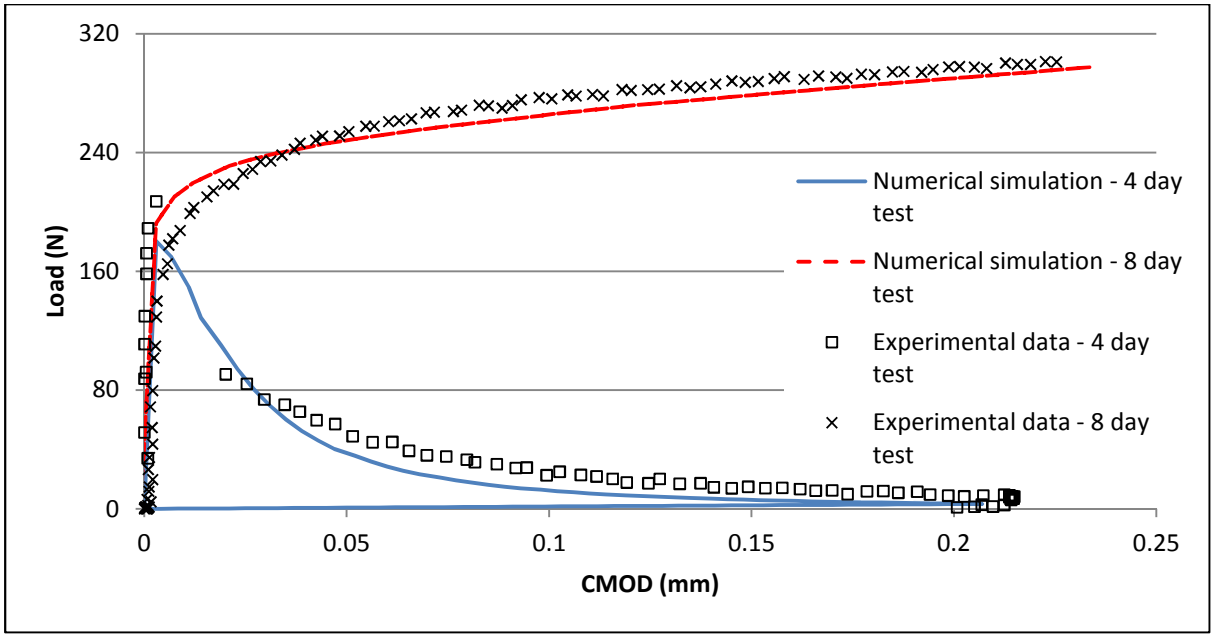

Figure 6 - Comparison between experimental data and numerical simulation predictions for example 1

3.2. Example 2

In this example, the nonlinear time-dependent beam model was used to analyse 12 singly reinforced concrete specimens tested by Gilbert [46]. Over a period of 400 days, the simply supported specimens were subjected to a constant sustained service load. A more detailed description of the tests and specimens can be found in reference [46]. The material parameters and geometric specimen data are given in Table 6 and Table 7 respectively. The creep parameters used for the FPZ element are shown in Table 5. A thermal strain corresponding to temperature values of T_1 = 10, and T_2 = 0, was applied on the third day after casting.

Table 6 – General material parameters for example 2

L (mm)	E (GPa)	f_c (MPa)	f_t (MPa)	E_s (GPa)	f_{yk} (MPa)	Φ (400 days)	ε_{sh} (400 days)	T_1 (°C)	T_2 (°C)	w_c (mm)	G_f (N/mm)
3500	22.82	18.3	2.57	200	500	1.71	0.000825	10	0	100	0.05

Note: G_f is a relatively low value for this example, however as the concrete was loaded at an early age (14 days) this is considered reasonable.

Table 7 – Individual specimen parameters for example 2

	Beams						Slabs					
Specimen	1a	1b	2a	2b	3a	3b	1a	1b	2a	2b	3a	3b
b (mm)	250	250	250	250	250	250	400	400	400	400	400	400
h (mm)	348	348	333	333	333	333	161	161	161	161	161	161
d (mm)	300	300	300	300	300	300	130	130	130	130	130	130
A_s (mm^2)	400	400	400	400	600	600	226	226	339	339	452	452
M_{ap}	24.90	17.00	24.80	16.80	34.60	20.80	6.81	5.28	9.87	6.81	11.40	8.34

A comparison between the predicted and measured 400 day deflections is given in Table 8. The predictions show good agreement, with a mean percentage difference of 12.46 %. The standard deviation is 8.54 % which, although apparently large, is considered within acceptable limits when taking into account the variability of concrete properties.

Table 8 – Example 2 – Results

		Beams						Slabs					
Specimen		1a	1b	2a	2b	3a	3b	1a	1b	2a	2b	3a	3b
400 day deflection (mm)	**Measured**	12.1	7.4	12.4	7.9	13.3	7.9	25.1	19.9	29.8	21.9	32.5	22.9
	Simulated	11.7	8.5	11.8	8.7	12.6	8.7	31.1	26.2	33.0	26.0	32.0	26.2
% difference		3.31	14.86	4.84	10.13	5.26	10.13	23.90	31.66	10.74	18.72	1.54	14.41
										Mean % difference			12.46
										Standard deviation			8.54

This agreement is considered to validate the numerical model's ability to take account of the time-dependent creep and shrinkage behaviour of the concrete, strains due to thermal contraction of the concrete, and the effects of cracking in both the continuum beam and FPZ elements on the load-deflection response.

4. LONG TERM SIMULATIONS

At present, no experimental tests have been developed to quantify the long term performance of the LCX system, thus predictions of the relevant behaviour will now be made using the model presented herein. Predictions from this model are expected to be useful in the future development of the system; both by guiding experimental studies, and aiding the design of reinforced concrete elements employing the LCX system.

The long term behaviour of two beam types has been simulated here in order to demonstrate the capabilities of the model and provide quantifiable predictions for the crack closure benefits of the LCX system.

Crack widths in this section are calculated from the product of the fracture strain for the bottom layer (ε_{fr}) and the FPZ width (w_c). The long term behaviour of each beam has been simulated for two different cases; a standard reinforced concrete section (SRC), and a section employing the LCX system; and the results quantitatively compared.

In each simulation, the beam's behaviour has been simulated for a period of 10 years, a period considered sufficient for trends to be reliably observed. In simulations including the LCX system; activation of the polymer occurs 28 days after casting, the polymer bars have an area equal to 2 % of the gross concrete area, and are positioned one third of the full concrete depth above the bottom face. Except for in the simulations referred to as LCX–100, and LCX–100–0.5 in Figure 8, the values of the material parameters used in the polymer constitutive model were taken from the work of Hazelwood et al [44] (see Table 9). Healing was only considered to have an effect in the LCX–100–0.5 simulation, thus in all other simulations parameter H was set to zero.

Table 9 – SMP material parameters

α	E_{TH}	E_p	T_{LE}	T_{HE}	b_p	d_p	σ_{res}

$10^{-4.8}$	845 MPa	6000 MPa	70°C	120°C	3.3	1.2	26.57 MPa
η_{2L}	η_{2H}	$T_{L\eta}$	$T_{H\eta}$	c_p	f_p	τ_p	β_R
1.575×10^4 P	3.122×10^7 P	30°C	90°C	5	0.1	2×10^5 s	0.98

Note: Some of the symbols names here have been changed from those used in the work of Hazelwood et al [44] due to the possibility of duplicate symbols within the present work.

All specimens from Example 2 have been analysed using the same parameters as those given in Table 5, Table 6, and Table 7; and described in the previous section relating to this example.

The full predicted behaviour of specimen B1a over the ten-year period is displayed in Figure 7 (this specimen was chosen due to the model's accuracy in predicting the 400 day deflection of this beam - see Table 8). The predicted ten-year crack widths for all specimens are displayed in Table 10.

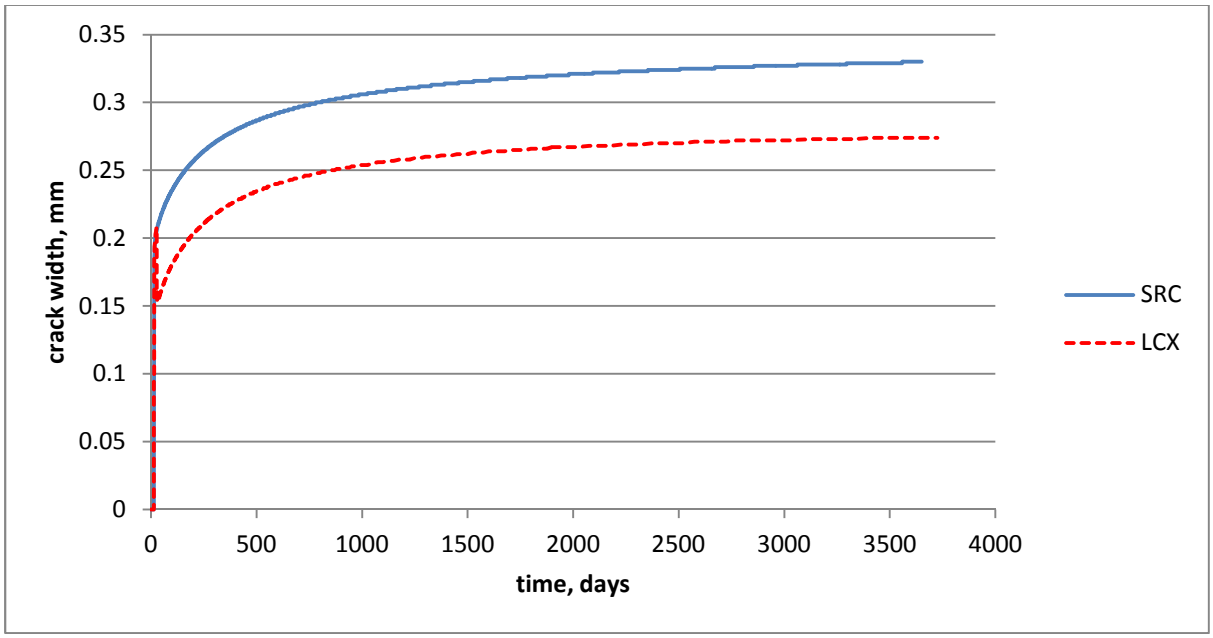

Figure 7 – Long term simulations of both RC and LCX behaviour for specimen B1a

The predicted crack width development with time for the SRC beam shown in Figure 7 is as expected. The shape of the curve for the LCX beam is similar, except that there is a sharp decrease in the crack width when the polymer is activated. After this point, the crack width

continues to increase at the same rate as observed in the SRC beam. Putting this into context; in the SRC beam, a ten-year crack width of approximately 0.33 mm is predicted, compared to a ten-year crack width of approximately 0.27 mm in the LCX beam; a 17.0 % reduction. These trends were consistently predicted for all beams analysed. The quantitative predictions for all 12 specimens are shown in Table 10.

Table 10 – Ten-year RC and LCX crack widths for all validation specimens

		Beams						Slabs					
Specimen		1a	1b	2a	2b	3a	3b	1a	1b	2a	2b	3a	3b
M_{ap}/M_u (%)		44.3	30.2	44.1	29.8	42.4	25.5	49.0	38.0	48.6	33.6	43	31.6
Ast/bd (%)		0.53	0.53	0.53	0.53	0.83	0.83	0.43	0.43	0.65	0.65	0.87	0.87
Crack width (mm)	**RC**	0.33	0.278	0.303	0.255	0.295	0.237	0.414	0.37	0.402	0.339	0.376	0.326
	LCX	0.269	0.218	0.252	0.203	0.261	0.203	0.321	0.276	0.339	0.276	0.329	0.279
% decrease		17.0	19.8	15.5	18.4	10.5	13.1	21.0	23.5	14.4	17.1	11.7	13.5
										Mean % decrease			16.3

Table 10 shows that, for the 12 long term comparisons considered, the percentage decrease in ten-year crack width ranges from a minimum of 10.5 % to a maximum of 23.5 %, with a mean of 16.3 %. Closer observation of the data presented in Table 10 reveals a trend of increasing crack width reduction with decreasing reinforcement as a percentage of gross concrete area. This trend occurs because any increase in reinforcement area causes an increase in damage to the cementitious matrix due to creep, shrinkage, and thermal effects as a result of the increased restraint. Providing the reinforcement has not been loaded beyond its elastic limit, the effectiveness of the SMP tendons is independent of the area of reinforcement present and thus, as a percentage, the crack width reduction is greater for beams with lower areas of reinforcement.

A second long term simulation has been carried out on a beam designed to Eurocode 2 [37]. The dimensions of the beam and applied loading have been chosen to be typical of an insitu RC beam in an office building. The design criteria for this beam are shown in Table 11.

Table 11 – Design criteria for Eurocode designed beam

Design life (years)	Exposure class	Span (m)	Live UDL (kN/m) (unfactored)	Dead UDL (kN/m) (unfactored)
50	XC1	5	9	22

The resulting beam dimensions and material properties used in the simulation are shown in Table 12. The material strengths for the steel and concrete properties have been taken as mean values, thus the predictions given below are assumed to represent the actual behaviour of a beam with averaged material parameters.

Table 12 – Model parameters for Eurocode designed beam

E (GPa)	f_c (MPa)	f_t (MPa)	E_s (GPa)	f_{yk} (MPa)	b (mm)	h (mm)	d (mm)	G_f (N/mm)
33	38	2.9	200	580	300	450	410	0.12
A_s (mm^2)	M_{ap} (kNm)	T_1 (℃)	T_2 (℃)	w_c (mm)	t_{TH} (days)	t_0 (days)	t_H (days)	
942	86.0	28	0	100	3	7	32	

The creep parameters applied to the FPZ element are shown in Table 5. A thermal strain corresponding to temperature values of T_1 = 28, and T_2 = 0, was applied on the third day after curing in this example (Equation (10)). These values were based on BD28/87 [47].

A predicted crack width of 0.271mm, due to quasi permanent loads, was calculated according to Eurocode 2 [37]. A long term simulation of this beam (assuming SRC) gave a fifty-year crack width of 0.234 mm. The 13.7% discrepancy is considered to be reasonable.

As well as the SRC simulation, three LCX simulations were carried out for this beam. The two additional simulations aimed to demonstrate the potential capability of a fully developed LCX system. The first of these is a simulation with identical polymer properties to those used in the above LCX simulations. In the second and third LCX simulations, the potential restrained shrinkage stress, σ_{res}, was been increased from 27 MPa to 100 MPa. The value of a 100MPa was based on the work of Long and Ward [48]. Furthermore, in the third LCX simulation, the healing parameter H was set to 0.5, which assumes that 50% of damage was healed. This percentage is considered to be a conservative estimate of the healing potential possible with certain polymeric based healing agents [25]. This 50 % healing was applied immediately after the activation of the polymer.

The results from the ten-year simulation for a standard reinforced concrete version and from the three LCX versions of the Eurocode beam are shown on Figure 8 with the three LCX simulations labelled LCX, LCX–100, and LCX-100–0.5 respectively.

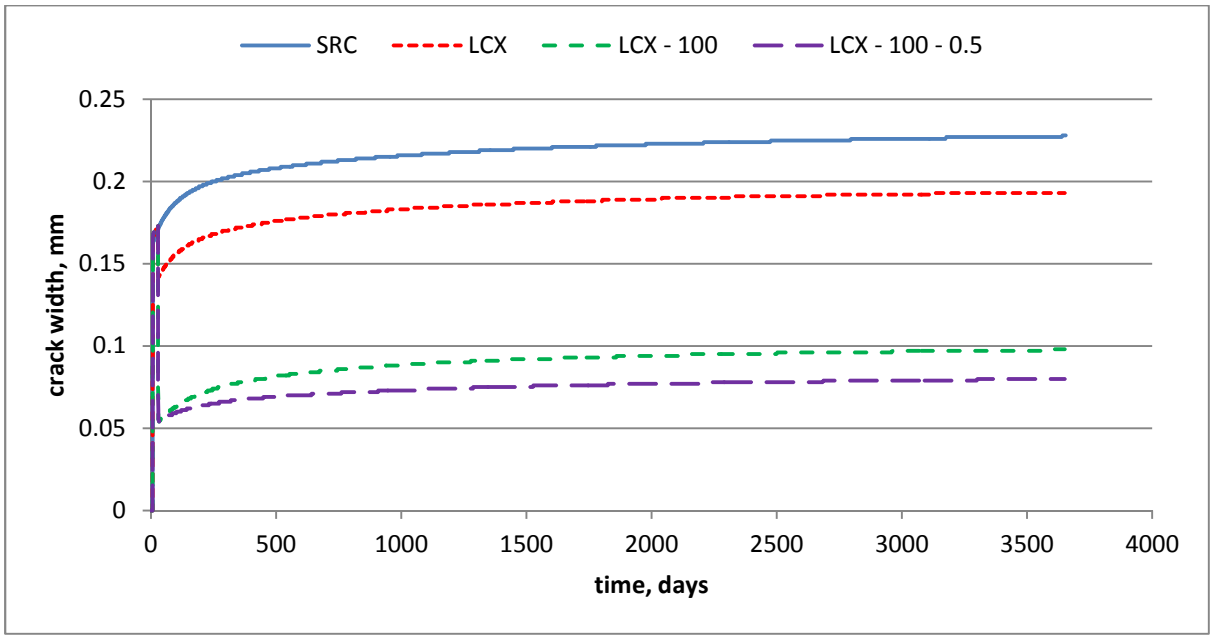

Figure 8 – Long term simulations of both RC and LCX behaviour for beam designed to Eurocode specification

Similar behaviour is observed for the SRC and LCX simulations in Figure 8 as that previously noted and described in Figure 7. The LCX–100, and LCX–100–0.5 simulations

show identical initial behaviour up to the point of activation. At this time, as would be expected, the crack closure is significantly greater (approximately 4 times) in the LCX-100 case than in the case of the LCX simulation with a σ_{res} value of 26.6 MPa. After activation, the crack width once again continues to grow with continued creep and shrinkage of the concrete. In the LCX–100–0.5 simulation, this growth occurs more slowly than in the LCX–100 simulation, as would be expected for a specimen in which 50 % of damage has been healed.

Figure 8 shows that, in the standard reinforced concrete beam, a ten-year crack width of approximately 0.23 mm is predicted, compared to a ten-year crack width of approximately 0.19 mm in the LCX beam; a 15.4 % decrease in crack width. The predicted ten-year crack for the LCX-100 case was 0.10 mm and 0.08 mm for the LCX–100–0.5 case, decreases of 57 % and 65 % respectively. Finally, it is noted that these latter shrinkage potential and healing values are expected to be realised in the near future.

4.1. Model sensitivity

Some sensitivity studies have been undertaken to ascertain which factors, if any, have a significant effect on the predictions of the model. The sensitivity of the SRC and LCX–100 simulations, displayed in Figure 8, to variations in the magnitude of the creep strain, shrinkage strain, and polymer relaxation has been assessed.

A 10 % increase in shrinkage strain increased the ten-year crack width by 2 % and 4 % in the SRC and LCX–100 beams respectively. This caused the predicted effectiveness of the LatConX system to decrease very slightly, with ten-year crack width reductions of 56 % compared to the baseline of 57 %.

A 10 % increase in creep strain increased the ten-year crack width by 8 % and 14 % in the SRC and LCX–100 beams respectively. This caused the predicted effectiveness of the LatConX system to decrease slightly more than in the shrinkage sensitivity just described, with ten-year crack width reductions of 54 % expected.

Finally, the most significant reduction in the predicted effectiveness of the LatConX system was found in the polymer relaxation sensitivity. A 10 % increase in the percentage of polymer stress subject to relaxation caused the ten-year crack width for the LCX–100 beam to increase by 14 %, this gives a 50 % reduction in ten-year crack width compared to the SRC beam. This is considered to be a highly pessimistic scenario and it is encouraging that significant reductions in crack width are still predicted.

5. CONCLUSION

A numerical study on the long-term behaviour of a novel self-healing cementitious composite material system, named LatConX, has been presented. A new numerical model is described that couples a layered beam model for the long-term behaviour of reinforced concrete beams with a thermo-mechanical transient model for shape memory polymer tendons. The coupled model has been validated using a range of experimental data.

Finally, a set of ten-year predictions for crack widths in standard reinforced concrete beams and beams employing the LatConX system have been compared. The long term simulations provide strong evidence for the potential effectiveness of the LatConX system in limiting crack widths in reinforced concrete structural elements. The results showed that a polymer with a shrinkage stress potential of 27MPa resulted in a 16.3% reduction in 10-year crack widths. However, the results also show that a 65% reduction is achievable when a polymer shrinkage stress of 100MPa is employed and 50% of the damage is healed. These latter figures are expected to be achievable in the near future.

Acknowledgements

Hazelwood would like to acknowledge the support and funding provided to him by the BRE & Presidents scholarship. The authors also acknowledge support for the work on self-healing systems from EPSRC grant Number EP/K026631/1, i.e. the M4L project.

Appendix A – Model algorithms

Creep

The creep strain is a function of both time and stress, thus it is different for each beam layer. The algorithm outlined details how the creep strain is computed for a single layer and is therefore run in full for each layer.

1	$\varepsilon_{prevcr} = \varepsilon_{cr}$	*Record current creep strains*
2	$\varepsilon_{cr} = 0$	*Reset ε_{cr} array to zeros*
3	if $(\varepsilon_{tot} - \varepsilon_{sh} - \varepsilon_{TH} - \varepsilon_{prevcr}) > 0$ $\varepsilon_{fr} = \omega(\zeta)^*(\varepsilon_{tot} - \varepsilon_{sh} - \varepsilon_{TH} - \varepsilon_{prevcr})$ otherwise $\varepsilon_{fr} = 0$	*Compute ε_{fr} to take account of any tensile creep* *See Equation (8).*
4	$\varepsilon_{efc} = \varepsilon_{tot} - \varepsilon_{sh} - \varepsilon_{TH} - \varepsilon_{fr}$	*Compute effective creep strain to be applied to creep model for current time step* *See Equation (7).*
5	for i = 2…4 $\varepsilon_{vec_{i_j}} = \varepsilon_{efc}\left(1 - e^{-\frac{\Delta t}{\tau_i}}\right) + \varepsilon_{vec_{i_{j-1}}}\left(e^{-\frac{\Delta t}{\tau_i}}\right)$ $\varepsilon_{cr} = \varepsilon_{cr} + \beta_i \varepsilon_{veci}$	*Compute viscoelastic strain for each dashpot and updated creep strain for each layer* *See Equations (6) and (9).*
6	$\Delta\varepsilon_{cr} = \varepsilon_{cr} - \varepsilon_{prevcr}$	*Compute change in creep strain for time step*

Shrinkage

Determining the shrinkage strain, ε_{sh}, is the simplest process as the strain is purely time-dependent and as such is the same for each beam layer.

1	$\Delta\varepsilon_{sh} = \varepsilon_{sh}(t) - \varepsilon_{sh}(t- \Delta t)$	*Compute change in shrinkage strain for time step*
2	$\varepsilon_{sh} = \varepsilon_{sh} + \Delta\varepsilon_{sh}$	*Update total shrinkage strain*

Polymer Functions

1	$\varepsilon_{ve1} = \varepsilon_R \left(1 - e^{-\frac{\Delta t}{\tau}}\right) + \varepsilon_{ve1_{prev}} \left(e^{-\frac{\Delta t}{\tau}}\right)$ $\varepsilon_{ve2} = \varepsilon_R \left(1 - e^{-\frac{\Delta t}{\tau(T)}}\right) + \varepsilon_{ve2_{prev}} \left(e^{-\frac{\Delta t}{\tau(T)}}\right)$	*Update viscoelastic strains*

Iterative Solver

1	ε_{bar}, θ_2, ε_L, ζ, ε_{LH}, ζ_H, T, M, ΔM, σ_p, ε_{sh}, $\Delta\varepsilon_{sh}$, ε_{cr}, $\Delta\varepsilon_{cr}$, ε_{TH}, $\Delta\varepsilon_{TH}$, ε_H, ω_H, H, ε_{ve1}, ε_{ve2}, ε_p	*Inputs from time dependent processes and current beam configuration*
2	$\zeta_{prev} = \zeta$, $\zeta_{Hprev} = \zeta_H$, $\psi = 10^{20}$, isec = 0, $\sigma_{prev} = \sigma_p$	*Initialise previous damage array, convergence parameter and tangent/secant matrix selector parameter*
3	$L_R = L + \Delta L_{FPZ} + \Delta L_{nle}$ $\varepsilon_R = \frac{L_R - L_{pmin}}{L_{pmin}}$ $\sigma_p = \beta \cdot E_1 \cdot \varepsilon_P + (1-\beta) \cdot E_1 \cdot (\varepsilon_P - \varepsilon_{ve1}) + E_2(T) \cdot (\varepsilon_P - \varepsilon_{ve2}) - \alpha \cdot \left(E_1 + E_2(T)\right) \cdot (T - T_{ambient})$ $\Delta\sigma_p = \sigma_p - \sigma_{prev}$	*Update polymer stress for updated viscous strains and compute change in polymer stress* *See Equations (13) - (17).*
4	while $\psi > 10^{-5}$	*Enter iterative loop*
5	$\Omega = \Omega_T(\varepsilon_{bar}, \theta_2, \zeta, \varepsilon_H, \omega_H, H, \zeta_H)$ $RHS = RHS\left(\Delta M, \Delta\sigma_p, \Delta\varepsilon_{sh}, \Delta\varepsilon_{cr}, \Delta\varepsilon_{TH}, \zeta, \varepsilon_H, \omega_H, H, \zeta_H, \varepsilon_{bar}, \theta_2\right)$	*Form stiffness matrix for nonlinear fracture zone and right hand side of equation*
6	$\begin{bmatrix} \Delta\varepsilon_{bar} \\ \Delta\theta_2 \end{bmatrix} = [\Omega]^{-1} * [RHS]$	*Solve system of equations*
7	$\varepsilon_{bar} = \varepsilon_{bar} + \Delta\varepsilon_{bar}$, $\theta_2 = \theta_2 + \Delta\theta_2$	*Add strain increments to current strain level*
8	$\varepsilon_L = \varepsilon_{bar} - 2\frac{\theta_2}{w_c} z_L - \varepsilon_{sh} - \varepsilon_{cr} - \varepsilon_{TH}$ $\zeta = max\left(0.999\varepsilon_t, \varepsilon_L, \zeta_{prev}\right)$ $\varepsilon_{LH} = \varepsilon_L - \varepsilon_H$ $\zeta_H = max\left(0.999\varepsilon_t, \varepsilon_{LH}, \zeta_{Hprev}\right)$	*Update layer data*
9	$\Psi_{prev} = \psi$ $\psi = RHS\left(M, \sigma_p, \varepsilon_{sh}, \varepsilon_{cr}, \varepsilon_{TH}, \zeta, \varepsilon_H, \omega_H, H, \zeta_H, \varepsilon_{bar}, \theta_2\right) - \Omega(\varepsilon_{bar}, \theta_2, \zeta, \varepsilon_H, \omega_H, H, \zeta_H)$	*Store previous convergence parameter, and compute current convergence.*
10	if $\psi - \Psi_{prev} > 0$ isec = 1	*Set tangent/secant matrix selector parameter*
11	if $\psi < 10^{-5}$	*Evaluate convergence and break if*

	Break return (ε_{bar}, θ_2, ζ, σ_p, ζ_H) else continue iterative procedure below	*converged*
12	RHS = ψ if isec = 0 $\Omega = \Omega_T(\varepsilon_{bar}, \theta_2, \zeta, \varepsilon_H, \omega_H, H, \zeta_H)$ else $\Omega = \Omega(\varepsilon_{bar}, \theta_2, \zeta, \varepsilon_H, \omega_H, H, \zeta_H)$	*Reform stiffness matrix for latest strains and damage parameters, RHS is the out of balance force from previous iteration*
13	while ψ > 10^{-5} Repeat steps 6 – 13	*Continue iterative process from step 6 onwards*

[1] Jefferson, A.D. et al. 2010. A new system for crack closure of cementitious materials using shrinkable polymers. *Cement and Concrete Research* 40(5) pp, 795–801.
[2] Kupfer, H.B. and Gerstle, K.H. 1973. Behavior of Concrete Under Biaxial Stresses. *ASCE Journal of Engineering Mechanics Division* 99(EM4), pp. 853–866.
[3] William, K.J. and Warnke, E.P. 1975. Constitutive models for triaxial behavior of concrete. *Proc Int Assoc Bridge Struct*. Engrg (Report 19), pp. 1–30.
[4] Chen, A.C.T and Chen, W.F. 1975. Constitutive Relations for Concrete. *ASCE Journal of Engineering Mechanics Division* 101(4), pp. 465–481.
[5] Etse, G. and Willam, K. 1994. Fracture energy formulation for inelastic behavior of plain concrete. *Journal of Engineering Mechanics* 120(9), pp. 1983–2011.
[6] Feenstra, P.H. and De Borst, R. 1995. A plasticity model and algorithm for mode-I cracking in concrete. *International Journal for Numerical Methods in Engineering* 38(15), pp. 2509–2529.
[7] Chen, W.F. 1996. *Plasticity in reinforced concrete*. Florida: J. Ross Publishing.
[8] Krajcinovic, D. 1996. *Damage mechanics*. Amsterdam ; New York: Elsevier.
[9] Mazars, J. 1986. A description of micro- and macroscale damage of concrete structures. *Engineering Fracture Mechanics* 25(5–6), pp. 729–737.
[10] Oliver, J. et al. 2002. From continuum mechanics to fracture mechanics: the strong discontinuity approach. *Engineering Fracture Mechanics* 69(2), pp. 113–136.
[11] Comi, C. and Perego, U. 2001. Fracture energy based bi-dissipative damage model for concrete. *International Journal of Solids and Structures* 38(36–37), pp. 6427–6454.
[12] Giry, C. et al. 2011. Stress-based nonlocal damage model. *International Journal of Solids and Structures* 48(25–26), pp. 3431–3443.
[13] Simo, J.C. and Ju, J. W. 1987. Strain- and stress-based continuum damage models-I. Formulation. *International Journal of Solids and Structures* 23(7), pp. 821–840.
[14] Carol, I. et al. 2002. An 'extended' volumetric/deviatoric formulation of anisotropic damage based on a pseudo-log rate. *Eur. J. Mech. - ASolids* 21(5), pp. 747–772.
[15] De Borst, R. and Gutiérrez, M. A. 1999. A unified framework for concrete damage and fracture models including size effects. *Int. J. Fract.*, 95(1–4), pp. 261–277.
[16] Desmorat, R. et al. 2007. Nonlocal anisotropic damage model and related computational aspects for quasi-brittle materials. *Engineering Fracture Mechanics* 74(10), pp. 1539–1560.
[17] Ortiz, M. 1985. A constitutive theory for the inelastic behavior of concrete. *Mech. Mater.*, 4(1), pp. 67–93.
[18] Lubliner, J. et al. 1989. A plastic-damage model for concrete. *International Journal of Solids and Structures* 25(3), pp. 299–326.
[19] Lee, J. and Fenves, G.L. 1998. Plastic-damage model for cyclic loading of concrete structures. *Journal of Engineering Mechanics* 124(8), pp. 892–900.
[20] Jefferson, A.D. 2003. Craft - A plastic-damage-contact model for concrete. I. Model theory and thermodynamic considerations. *International Journal of Solids and Structure*s 40(22), pp. 5973–5999.
[21] Jason, L. et al. 2006. An elastic plastic damage formulation for concrete: Application to elementary tests and comparison with an isotropic damage model. *Comput. Methods Appl. Mech. Eng.* 195(52), pp. 7077–7092.
[22] Grassl, P. and Jirásek, M. 2006. Damage-plastic model for concrete failure. *International Journal of Solids and Structures* 43(22–23), pp. 7166–7196.
[23] Joseph, C. et al. 2011. Self-healing cementitious materials: A review of recent work. *Proc. Inst. Civ. Eng. Constr. Mater.* 164(1), pp. 29–41.
[24] Wu, M. et al. 2012. A review: Self-healing in cementitious materials and engineered cementitious composite as a self-healing material. *Construction and Building Materials* 28(1), pp. 571–583.
[25] Van Tittelboom, K. and De Belie, N. 2013. Self-healing in cementitious materials-a review. *Materials* 6(6), pp. 2182–2217.

[26] Miao, S. et al. 1995. Constitutive models for healing of materials with application to compaction of crushed rock salt. *Journal of Engineering Mechanics* 121(10), pp. 1122–1129.
[27] Mergheim, J. and Steinmann, P. 2013. Phenomenological modelling of self-healing polymers based on integrated healing agents. *Computational Mechanics* 52(3), pp. 681–692.
[28] Barbero, E.J. et al. 2005. Continuum Damage-healing Mechanics with Application to Self-healing Composites. *International Journal of Damage Mechanics* 14(1), pp. 51–81.
[29] Schimmel, E.C. and Remmers, J.J.C. 2006. *Development of a constitutive model for self-healing materials*. Delft Aerospace Computational Science.
[30] Voyiadjis, G.Z. et al. 2011. A thermodynamic consistent damage and healing model for self healing materials. *International Journal of Plasticity* 27(7), pp. 1025–1044.
[31] Bažant, Z.P. 2001. Prediction of concrete creep and shrinkage: past, present and future. *Nucl. Eng. Des.* 203(1), pp. 27–38.
[32] American Concrete Institute (ACI). 1982. Prediction of creep, shrinkage, and temperature effects in concrete structures. *ACI Comm.* 209.
[33] Bažant, Z.P. and Baweja, S. 1995. Creep and shrinkage prediction model for analysis and design of concrete structures- model B3, *Mater. Struct.* 28(6), pp. 357–365.
[34] Wendner, R. et al.2013. The B4 model for multi-decade creep and shrinkage prediction. In Proceedings of Ninth International Conference on Creep, Shrinkage, and Durability Mechanics (CONCREEP-9). Cambridge, Massachusetts 22-25 September 2013. Virginia: American Society of Civil Engineers pp. 429–436.
[35] CEB-FIP, *CEB-FIP model code 1990: Design code*. London: Thomas Telford, 1994.
[36] Gardner, N.J. and Lockman, M.J. 2002. Design provisions for drying shrinkage and creep of normal-strength concrete. *ACI Materials Journal* 99(1), pp. 111–112.
[37] BSI, *BS EN 1992-1-1:2004 Eurocode 2: Design of concrete structures - Part 1-1: General rules and rules for buildings*. London, UK: BSI, 2004.
[38] Goel, R. et al. 2007. Comparative study of various creep and shrinkage prediction models for concrete. *J. Mater. Civ. Eng.* 19(3), pp. 249–260.
[39] Bažant, Z.P. and Prasannan, S. 1989 Solidification theory for concrete creep I. Formulation. *Journal of Engineering Mechanics* 115(8), pp. 1691–1703.
[40] Bažant, Z.P. et al. 1997. Microprestress-solidification theory for concrete creep. I: Aging and drying effects. *Journal of Engineering Mechanics* 123(11), pp. 1188–1194.
[41] Jefferson, A.D. et al. 2014. Finite element crack width computations with a thermo-hygro-mechanical- hydration model for concrete structures. *European Journal of Environmental Civil Engineering* 18(7), pp. 793–813.
[42] Bažant Z. P. and Oh, B. H. 1983. Crack band theory for fracture of concrete. *Mater. Struct.* 16 pp. 155–177.
[43] Beeby, A.W. and Scott, R.H. 2005. Cracking and deformation of axially reinforced members subjected to pure tension. *Magazine of Concrete Research* (57)10, pp. 611–621.
[44] Hazelwood, T. et al. 2014. Long-term stress relaxation behaviour of predrawn poly(ethylene terephthalate). *Journal of Applied Polymer Science* 131(23).
[45] Dunn, S.C. et al. 2011. Shrinkage behaviour of poly(ethylene terephthalate) for a new cementitious-shrinkable polymer material system. *Journal of Applied Polymer Science* 120(5), pp. 2516–2526.
[46] Gilbert, R.I. 2013. Time-dependent stiffness of cracked reinforced and composite concrete slabs. *Procedia Engineering* 57, pp. 19–34.
[47] The Highways Agency, *BD 28/87 Early Thermal Cracking of Concrete*. 1987.
[48] Long, S.D. and Ward, I.M. 1991. Shrinkage force studies of oriented polyethylene terephthalate. *Journal of Applied Polymer Science* (42)7, pp. 1921–1929.